

Chain Dynamics and Strain-Induced Crystallization of Pre- and Postvulcanized Natural Rubber Latex Using Proton Multiple Quantum NMR and Uniaxial Deformation by *in Situ* Synchrotron X-ray Diffraction

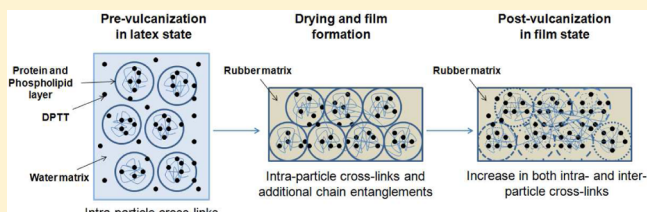
Justin Che,[†] Shigeyuki Toki,^{*,†} Juan L. Valentin,^{*,‡} Justo Brasero,[‡] Adun Nimpaiboon,^{‡,§} Lixia Rong,[†] and Benjamin S. Hsiao[†]

[†]Department of Chemistry, Stony Brook University, Stony Brook, New York, 11794-3400, United States

[‡]Instituto de Ciencia y Tecnología de Polímeros (CSIC), Madrid 28006, Spain

[§]Department of Chemistry and Center of Excellence for Innovation in Chemistry, Faculty of Science, Mahidol University, Bangkok 10400, Thailand

ABSTRACT: The structural development and morphology in unvulcanized and vulcanized (both pre- and postvulcanized) natural rubber latex were studied in a relaxed state and under deformation by multiple-quantum (MQ) NMR and *in situ* wide-angle X-ray diffraction (WAXD), respectively. Vulcanization was carried out using both sulfur and peroxide, showing important differences on the spatial distribution of cross-links according to the source of vulcanizing agents. Sulfur prevulcanization promotes the formation of highly homogeneous networks in the dispersed rubber particles, whereas peroxide vulcanization makes broader spatial cross-link distributions. The latter is compatible with the formation of core–shell network structures. Molecular orientation and strain-induced crystallization were analyzed by both stress–strain relations and WAXD. An increase in the vulcanizing agent concentration led to an increase in modulus and crystalline fractions. For sulfur vulcanization, the additional heat treatment (postvulcanization) increased the interactions between rubber particles and unreacted vulcanizing agents. For peroxide vulcanization, the additional heat treatment led to chain scission reactions and degradation of network points.



INTRODUCTION

Vulcanized rubber has been a subject of intensive research interest since the 1940s.^{1,2} However, it is only recently that natural rubber latex has gained significant research interest in the rubber industry. It has been well-known that natural rubber has superior strength as compared to synthetic rubber. In order to fully synthesize a rubber that can resemble the mechanical properties of natural rubber, it is essential to begin at the fundamentals and start at the rubber latex state.

Natural rubber latex is defined as the stable colloidal dispersion of polymeric particles (typically a few hundred nanometers in diameter) in an aqueous medium³ or simply “rubber particles in water”. Rubber latex is derived from the sap of the *Hevea Brasiliensis* tree.⁴ Latex is usually composed of 30–40% rubber particles, 55–65% water, and about 6% nonrubber components, including proteins, fatty acids, phospholipids, etc. According to Amnuayponsri et al.,⁵ proteins and phospholipids create the outside layer of the rubber particles, and the rubber chain molecules are located inside those particles.

Prevulcanization, drying/water evaporation (or film formation), and postvulcanization are the most important processes in the rubber industry. They modify the rubber network structure and define their overall mechanical proper-

ties. Therefore, it is necessary to understand what truly happens during these processes in order to correlate network structure with the physical properties of rubber. In prevulcanization, it has been postulated that the process takes place inside the rubber particles that are dispersed in water.³ A homogeneous solution containing natural rubber latex, activators, cure agents, antioxidants, and surfactants is mixed altogether. Vulcanization of rubber particles occurs inside each individual rubber particle, creating independent and nonconnected cross-linked rubber particles (with a given network structure inside the rubber particle) dispersed in water. After prevulcanization, water is removed, and the previously cross-linked particles become closer until they interact forming a coherent film. In postvulcanization, excess chemicals and water-soluble proteins are further removed by heating up the films at high temperatures. The mechanism of each of these states is the main focus of this paper and will be analyzed using double-quantum (DQ) NMR (more generally referred to as multiple-

Received: April 4, 2012

Revised: July 24, 2012

Published: August 1, 2012

Table 1. Recipes and Curing Conditions for Rubber Latex Samples Vulcanized with DPTT

	latex	latex post-heat treatment	latex DPTT 0.5	latex DPTT 1.0	latex DPTT 1.5	latex DPTT 0.5 PostV	latex DPTT 1.0 PostV	latex DPTT 1.5 PostV
prevulcanization (cure time)	no	no	yes (18 h)	yes (15 h)	yes (11 h)	yes (18 h)	yes (15 h)	yes (11 h)
postvulcanization (cure time)	no	yes (30 min)	no	no	no	yes (30 min)	yes (30 min)	yes (30 min)
DPTT, phr	no	no	0.75	1.50	2.25	0.75	1.50	2.25
ZnO, phr	no	no	0.30	0.60	0.90	0.30	0.60	0.90
Wingstay-L, phr	no	no	0.23	0.47	0.70	0.23	0.47	0.70
dispersants	no	no				potassium caprilate, casein, Darvan 1, KOH		

Table 2. Recipes and Curing Conditions for Rubber Latex Samples Vulcanized with Peroxide

	latex peroxide 0.6	latex peroxide 1.2	latex peroxide 1.8	latex per 0.6 PostV	latex per 1.2 PostV	latex per 1.8 PostV
prevulcanization (cure time)				yes (3 h)		
postvulcanization (cure time)	no	no	no	yes (30 min)	yes (30 min)	yes (30 min)
tert-butyl hydroperoxide, phr	0.60	1.20	1.80	0.60	1.20	1.80
activators			iron(III), fructose			
Wingstay-L, phr			no			
dispersants			potassium caprilate			

quantum (MQ) NMR) and wide-angle X-ray diffraction (WAXD).

DQ NMR is a powerful tool that can provide quantitative information regarding polymer network structure. More specifically, DQ NMR experiments are sensitive to the residual dipolar couplings (RDC) and their distributions, which can yield information on the number of cross-links and the spatial cross-links distribution. The existence of residual dipolar couplings (when the polymer is far away its characteristic T_g) on polymer networks is due to the presence of cross-links and entanglements that restrict fast segmental fluctuations, leading to nonisotropic orientation fluctuations that can be detected by using DQ experiments.⁶ The specific details of this procedure and analysis are discussed elsewhere.^{6–8}

Deformation along with *in situ* synchrotron X-ray scattering has been recently used to study the development of molecular structures in rubber. It has been well demonstrated that the roles of both molecular orientation and strain-induced crystallization are primarily responsible for the outstanding mechanical properties in natural rubber. The inhomogeneity of cross-linked topology in vulcanized natural rubber leads to a microfibrillar structure composed of crystalline segments between the cross-links (vulcanized points) during stretching.¹ The objective of this presented work is to study the structural development in unvulcanized and vulcanized natural rubber latex in a relaxed state and under deformation by DQ NMR and synchrotron X-rays in both pre- and postvulcanization states. DQ NMR studies the fluctuations of molecules at more local length scales, whereas synchrotron X-rays can analyze network structures at much larger length scales. The combination of both of these techniques can provide a considerable amount of information regarding rubber network structure.

EXPERIMENTAL SECTION

Rubber Latex Samples. Recipes and cure conditions for rubber latex samples vulcanized with sulfur and peroxide are listed in Tables 1 and 2, respectively. There were a total of 14 samples: latex, latex with heat treatment at 130 °C for 30 min, both sulfur and peroxide vulcanized latex at 60 °C for several hours depending on each sample's cure time (so-called prevulcanization), and samples that after several hours of prevulcanization and the subsequent film formation were submitted to an additional heating step at 130 °C for 30 min (so-called

postvulcanization). For each sample, the optimum prevulcanization time (in latex state) was determined by using proton multiple-quantum NMR (MQ NMR) spectroscopy carried out in an inexpensive low-field spectrometer.⁸

Dipentamethylenethiuram tetrasulfide (DPTT) was used as the sulfur source for vulcanization at three different concentrations: 0.75, 1.50, and 2.25 parts per hundred of rubber (phr) (denoted as DPTT 0.5, 1.0, and 1.5 for prevulcanized latex and 0.5, 1.0, and 1.5 PostV for postvulcanized latex, respectively). DPTT is an accelerator that has very active sulfur groups and good heat resistance. It is an excellent vulcanizing agent for latex.⁹

For prevulcanized latex with DPTT, a homogeneous dispersion containing natural rubber latex, activator (ZnO), cure agent (DPTT), antioxidant, and dispersants is mechanically stirred together during the prevulcanization process. A commercial antioxidant named Wingstay-L was used to prevent the high-temperature degradation of latex samples. The surfactants such as casein, Darvan 1, and potassium hydroxide were used to obtain a stable dispersion of DPTT, ZnO, and antioxidant in water, whereas potassium caprilate gives better mechanical stability. The resulting dispersion was then stirred and heated at 60 °C for various hours, depending on the sample's cure time, in order to vulcanize the individual rubber particles dispersed in water. Subsequently the prevulcanized samples were poured onto a glass Petri dish, and the dispersion was dried overnight at room temperature, allowing further removal of water and film formation. However, some water still remains in the film, but in very small quantities. After a few days, the weight of the film was constant. Preparation of postvulcanized samples included, after prevulcanization reaction and film formation, an additional heating at 130 °C for 30 min. The thicknesses of all the films were around 1 mm after water evaporation.

Pre- and postvulcanized latex with peroxide samples were prepared with the same methodology described previously. tert-Butyl hydroperoxide was used as the peroxide vulcanizing agent at three different concentrations: 0.6, 1.2, and 1.8 phr (denoted as peroxide 0.6, 1.2, and 1.8 for prevulcanized latex and peroxide 0.6, 1.2, and 1.8 PostV for postvulcanized latex, respectively). Activators and dispersants, including iron(III), fructose, and potassium caprilate, were used to prepare these samples. No antioxidants were added to the peroxide vulcanized samples.

For unvulcanized latex and latex with post-heat treatment, no additives were mixed with the samples. The only difference between these two samples was that latex after film formation underwent an additional heat treatment at 130 °C in order to compare it with the postvulcanized samples. Both of these samples served as a control.

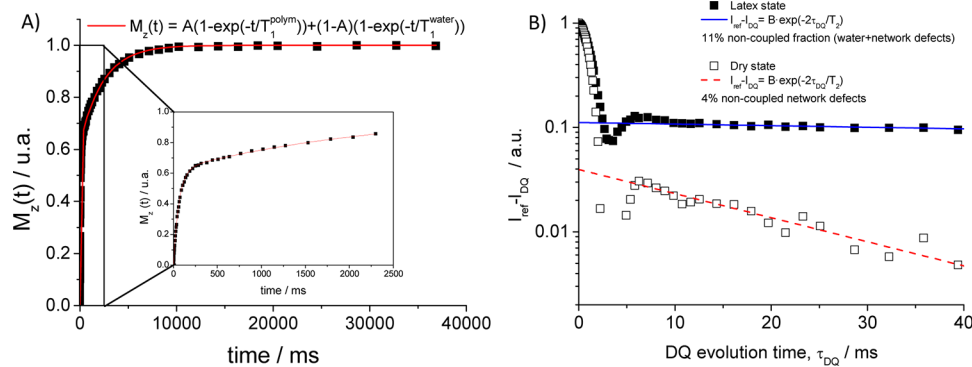


Figure 1. (A) Saturation recovery curve for latex state NR sample. Double-exponential fits, where $M_z(t)$ is the longitudinal magnetization at the experiment time t and A represents the fraction of sample with solidlike behavior, were used to analyze the curves. (B) Identification and subtraction of noncoupled fraction tails in a latex sample after and before drying. In the latex samples, the noncoupled fraction is mainly composed by water (i.e., the small fraction of water that was magnetized caused by the short rd used in the experiments) and nonelastic network defects, whereas in dry samples, the slowly relaxed tails are mainly related with network defects.

Time-Domain NMR Measurements. Different time-domain proton NMR experiments under static conditions were carried out at 60 °C (the optimum temperature for the analyzed samples) on a Bruker minispec mq20 spectrometer operating at 0.5 T with 90° pulses of 3 μ s length and dead time of 11 μ s.

Saturation Recovery Experiments. Recycle delay time for all experiments was always fixed as rd = $5T_1^{\text{polym}}$, where T_1^{polym} is the spin-lattice relaxation time of the polymer as measured by saturation recovery experiments. This followed the same experimental procedure that was used to characterize hydrogels¹⁰ because of its similarity with latex. This analysis (see Figure 1A) is important in rubber latexes because it allows the quantitative characterization of solidlike fractions (characterized by shorter spin-lattice relaxation time, $T_1^{\text{polym}} \sim 100$ ms) dispersed in the liquid media (e.g., water with $T_1^{\text{water}} \sim 2500$ ms). As a consequence, this method could be considered a potential tool to be used in quality control measurements in the latex industry to more quickly (around 20 min) analyze the rubber content in latexes.

^1H DQ-NMR Experiments. Study of Permanent Network Structure. ^1H DQ NMR experiments, based on enhanced Baum-Pines pulse sequences widely described elsewhere,⁶ were used to study the network structures of all samples in three different stages and states: prevulcanization in latex state, drying and film formation, and postvulcanization. In order to analyze the network structure of rubber samples, the raw experimental data need to be normalized in a way that the temperature-independent network structure effect (at temperatures far above the glass transition temperature) can be separated from the temperature-dependent segmental dynamics. The initial raw data includes plots of the DQ buildup (I_{DQ}) and reference decay (I_{ref}) as a function of the DQ evolution time (τ_{DQ}). The sum of both components ($I_{\text{DQ}} + I_{\text{ref}}$) gives the full magnetization of the sample, which includes signals from dipolar coupled network segments (segments between constraints) and uncoupled isotropic mobile protons. Identification of both contributions is quite easy since coupled network segments typically relax faster than noncoupled protons (see Figure 1B). It is important to remark on the special characteristics of latex samples with respect to the usually analyzed rubber (in dry state) samples. Rubber networks usually contain nonelastic network defects (mainly dangling chains and loops), which are mainly responsible for the noncoupled slowly relaxing tails in DQ experiments. In latex samples, rubber particles are dispersed in a water media, and therefore the noncoupled fraction of protons should be mainly composed of water (and small molecules dissolved or dispersed), which relax even slower than the nonelastic network defects. These tails were perfectly defined by a single-exponential function, and after its subtraction, no evidence of additional noncoupled tails was observed.

Subtraction of the long-time contribution of the noncoupled fraction is needed to obtain the total MQ magnetization ($I_{\Sigma\text{MQ}}$) from the coupled segments (eq 1), which is dependent on chain dynamics:

$$I_{\Sigma\text{MQ}} = I_{\text{DQ}} + I_{\text{ref}} - Be^{-2\tau/T_2} \quad (1)$$

where B is the noncoupled fraction of polymer chains and T_2 is the slow exponential decay factor of the noncoupled protons. The normalized DQ intensity ($I_{n\text{DQ}}$) is obtained by taking the ratio of the DQ intensity with respect to the total MQ magnetization (eq 2):

$$I_{n\text{DQ}} = I_{\text{DQ}} / I_{\Sigma\text{MQ}} \quad (2)$$

This latter equation depends on the residual dipolar couplings (D_{res}), which reflects the long-time anisotropy arising from cross-links and topological constraints.^{11,12}

The proper analysis of $I_{n\text{DQ}}$ provides quantitative information about the residual dipolar couplings (D_{res}) and their distribution. It was previously demonstrated^{6,7} that an assumption of a Gaussian distribution of dipolar couplings is a robust and good approach for analyzing the cross-linked NR and BR samples:

$$I_{n\text{DQ}}(D_{\text{res}}, \sigma_G) = \frac{1}{2} \left(1 - \frac{\exp \left\{ -\frac{\frac{2}{5}D_{\text{res}}^2 \tau_{\text{DQ}}^2}{1 + \frac{4}{5}\sigma_{\text{res}}^2 \tau_{\text{DQ}}^2} \right\}}{\sqrt{1 + \frac{4}{5}\sigma_G^2 \tau_{\text{DQ}}^2}} \right) \quad (3)$$

where D_{res} is the average apparent residual dipolar coupling (in units of rad/s) and σ is its standard deviation that characterizes the distribution width. From D_{res} , the molecular weight between constraints, M_c , can be determined for NR samples by

$$M_c^{(\text{NR})} = \frac{617 \text{ Hz}}{D_{\text{res}}/2\pi} \text{ kg/mol} \quad (4)$$

In consequence, the cross-link density, ν , for 4-functional cross-links can be determined by

$$\nu_{\text{NMR}} = \frac{1}{2M_c} \quad (5)$$

Finally, an improved numerical inversion procedure based on fast Tikhonov regularization was used to determine the actual dipolar coupling distribution. The modified version of the numerical fit, which was described in a recent paper,⁸ provides a reliable, precise, and quantitative picture of the actual distribution function of residual couplings, i.e., cross-links.

Study of Vulcanization Kinetics. According to the previously explained statements, this experimental methodology is useful to quantitatively evaluate the invariant network structures of vulcanized samples (in latex or solid state), but it is not applicable to networks under evolution in the experimental time scale, e.g., rubber networks during the vulcanization process. In order to analyze the

prevulcanization kinetics (in latex state), a faster but still quantitative modification of the DQ method was used.

This method, which was previously used to analyze gelation kinetics,¹³ involves the evaluation of I_{nDQ} in a single DQ time (an experimental time around 1 min) instead of the measurement of full DQ evolution time that needs longer measurement times (around 1 h according to the experimental settings used in this work). For the most sensitive single-point measurement, τ_{DQ} should be selected for which I_{nDQ} or I_{DQ} attains its highest values in the fully vulcanized sample with the highest cross-link density. For a more robust and conservative analysis, the time was selected close to but before the maximum. Taking into consideration these statements, the best DQ time for single-point detection was selected at 2.2 ms in order to study the prevulcanization kinetics in latex state.

Synchrotron X-ray and Tensile Measurements. Wide-angle X-ray diffraction (WAXD) measurements were carried out at the X27C beamline in the National Synchrotron Light Source (NSLS), Brookhaven National Laboratory (BNL). The X-ray wavelength was set at 1.371 Å. Two-dimensional (2D) WAXD patterns were acquired using a MAR-CCD detector. The typical image acquisition time for each scan was 30 s. Al₂O₃ was used to calibrate the scattering angle in WAXD, and the sample-to-detector distance was 124 mm. X-ray measurements for all samples were taken under the same conditions. All diffraction signals were corrected for beam fluctuations, sample absorption, and background scattering. Data analysis was performed using the software Polar (Stony Brook Technology and Applied Research, Stony Brook, NY).

Rubber latex cast samples were pre-cut into a dumbbell-like shape and clamped onto a tensile stretching device. This device allowed symmetric deformation of the sample and monitoring the structure change of the sample by illuminating the same sample position during deformation. The samples were deformed to strains up to 6.4 and relaxed back to stress of 0. The deformation rate was 10 mm/min and was carried out at room temperature. The initial strain rate is 0.005 S6 s⁻¹ (or 0.333 min⁻¹). Time-resolved WAXD patterns during deformation and stress-strain relations were recorded simultaneously. The stress is defined as load divided by original cross section. The strain is defined as the distance of the two clamps divided by original length.

Quantitative evaluations of mass fractions of crystals were determined for all of the samples based on the integrated intensity patterns. The corrected WAXD patterns prior to stretching at strain 0 contain only an isotropic amorphous halo with no preferred orientation. With increasing strain values, crystalline reflections started to develop and WAXD patterns began to contain both crystalline peaks and the amorphous halo (both oriented and unoriented). The total molecules at the stretched state contain both the isotropic and anisotropic contributions as shown in the following equations:

$$I(\text{total}) = I(\text{isotropic}) + I(\text{anisotropic}) \quad (6)$$

$$I(\text{isotropic}) = I(\text{unoriented amorphous}) \quad (7)$$

$$I(\text{anisotropic}) = I(\text{oriented amorphous}) + I(\text{oriented crystalline}) \quad (8)$$

The isotropic and anisotropic contributions in these patterns can be deconvoluted using the analytical method described by Toki et al.^{1,2} The isotropic contribution of the WAXD patterns at the stretched state showed a similar feature to the WAXD pattern at strain 0. The deconvoluted anisotropic contribution of the WAXD pattern could be composed of oriented crystalline reflections and an oriented amorphous phase. Two-dimensional peak-fit software was used to fit all the crystal peaks and the amorphous halo. The mass fraction of strain-induced crystals was quantitatively determined by taking the ratio of the integrated crystal areas with the total integrated area.

RESULTS AND DISCUSSION

¹H Double-Quantum (DQ) Solid-State NMR. Prevulcanization Kinetics. Vulcanization kinetics is followed in rubber

science and technology from the rheometer curves. Prevulcanization kinetics in NR latex cannot be measured by this methodology because it is dispersed in water. For that reason, this important step is usually indirectly studied by tedious mechanical measurements; i.e., samples prevulcanized at different times are dried, and the tensile strengths for the obtained films are tested.

In this sense, application of time domain NMR is a step forward to the study of prevulcanization kinetics providing important benefits for both industrial and academic applications. Prevulcanization takes place inside the NMR spectrometer at the desired temperature, and the experimental method allowed us to observe *in situ* how the intensity measured at a single DQ evolution time increases with the prevulcanization time due to the formation of cross-links (Figure 2). The shape of the prevulcanization process from the NMR measurements is quite similar to those obtained from the rheometer in "dry" rubber samples.¹⁴

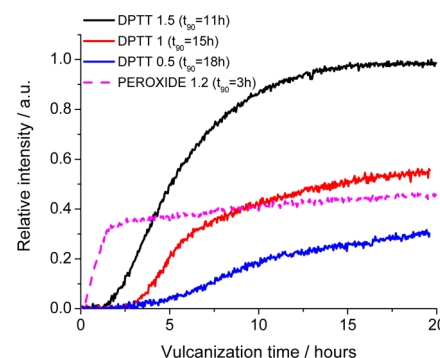


Figure 2. Relative intensity at the selected DQ evolution time of 2.2 ms as a function of vulcanization time for various concentrations of DPTT. The 1.2 phr peroxide vulcanized sample is also shown. The optimum vulcanization time (t_{90}) is shown in parentheses for each sample.

Samples vulcanized with DPTT show a scorch time where the accelerator chemistry takes place leading to the formation of the active sulfating agents but without the formation of cross-links. The second stage comprises the "chemistry of cross-linking", which includes reactions leading to the formation of cross-links and the fast increment on the NMR signal. It is important to note that all studied samples do not show a clear plateau which indicates the end of the reaction. This is because the prevulcanization reaction depends on two competing processes, i.e., the diffusion of chemicals inside the rubber particles and their reactions to create cross-links. As the cross-linking reaction takes place, the diffusion mechanism is limited, and the excess of the vulcanizing agent reacts slowly. These two competing processes will have an important impact on the network structure of each individual particle formed during the prevulcanization step, as will be discussed in the next sections. Nevertheless, it is clear that relative intensity increases with concentration of DPTT, which is indicative of an increase in cross-linking density.

Figure 2 also shows the relative intensity for the 1.2 phr peroxide vulcanized sample (other peroxide samples show almost identical behavior, and they were not included in Figure 2). Vulcanization with peroxide is based on radical reactions. After thermal decomposition of peroxide, the formed radicals react with the polymer backbone and, subsequently, cross-links

between polymer chains are created. This reaction pathway is so fast that it prevents the existence of scorch time. The reaction rates in sulfur vulcanized samples are much slower than peroxide vulcanized samples. The optimum vulcanization time (fixed as time for 90% conversion after 20 h of reaction, t_{90}) for DPTT 0.5, 1.0, and 1.5 were 18, 15, and 11 h, respectively, whereas samples vulcanized with peroxide were all 3 h.

Rubber Network Structure. Following the usual manufacturing procedure, after prevulcanizing the NR latex at their optimum time (obtained from NMR analysis, see Figure 2), a rubber film was made by drying the water. Finally, the films were thermally treated in the so-named postvulcanization process. In all cases, DQ NMR methodology was used to analyze the evolution on the network structure through the three different states.

Noncoupled Network Defects. Figure 3 shows the fraction of noncoupled network defects for the different samples in the

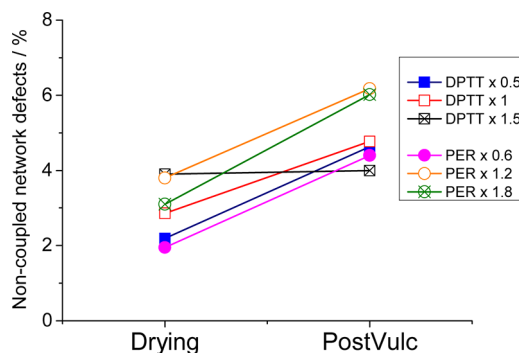


Figure 3. Percentage of noncoupled network defects in each state for the studied samples.

different states. It is important to point out that prevulcanized samples in the latex state do not present any measurable noncoupled network defects, whereas they emerge (although in small fractions) after film formation and postvulcanization.

Weak (albeit systematic) variations, between 2% and 6% in fraction of noncoupled network defect after the postvulcanization process, were observed. This could be related with degradative processes promoted in this step, as will be discussed in the next sections.

Prevulcanization Process. In previous works,^{6,7} the advantages of applying DQ NMR experiments for the complete analysis of rubber network structure, i.e., cross-link density and

spatial distribution of cross-links, were pointed out. Nevertheless, in latex samples this methodology is even more important since it allows the study of rubber network structure in the latex state. It is an unresolved experimental challenge in this field, since well-established experimental methodologies for the analysis of cross-link density, e.g., equilibrium swelling experiments, uniaxial tensile strength, etc., are only applicable to dried samples.

Figure 4A shows the cross-linking density measured by NMR of various samples in the three different states. We can clearly see that the cross-linking density increases with concentration of DPTT in all three different states. Furthermore, at each concentration of DPTT, the cross-linking density for drying and postvulcanization in the film state is higher than the cross-linking density for prevulcanization in the latex state.

These results demonstrate that conventional experimental methods for the analysis of rubber network structures just give information about the global process, e.g. the effect of prevulcanization and film formation on the rubber network structure. On the opposite hand, NMR spectroscopy is able to separate and independently analyze each individual step. In this sense, NMR results after prevulcanization reflect the network structure of the individual cross-linked rubber particles dispersed in water. They are direct experimental evidence about the effect of prevulcanization reaction without any disturbance caused by additional procedures. A linear relationship between cross-link density and concentration of vulcanizing agents was found (see Figure 4B). In DPTT vulcanization, only the two central sulfur atoms are able to create cross-links. It means that the maximum efficiency on vulcanization reaction should be 2 mol of cross-links (composed exclusively by monosulfidic bridges) per mole of DPTT. According to the slopes in Figure 4B, the reaction efficiency during the prevulcanization process is close to unity. This could be related to the formation of larger sulfidic cross-links (if a complete reaction of DPTT is supposed) or just by a partial reaction of DPTT. The latter emerged as the most reliable factor, as will be discussed later in this section. Finally, it is important to note that the spatial distribution of cross-links (measured as variation of the relative width of the distribution of cross-link density (σ) to the average value (D_{res}) assuming a Gaussian distribution of cross-links) became more homogeneous with the increase in amount of DPTT (Figure 5).

A different scenario takes place when peroxide was used as the vulcanizing agent. The reaction efficiency is very low, and the addition of increased amounts of peroxide does not create additional cross-links, at least in the expected amount. To

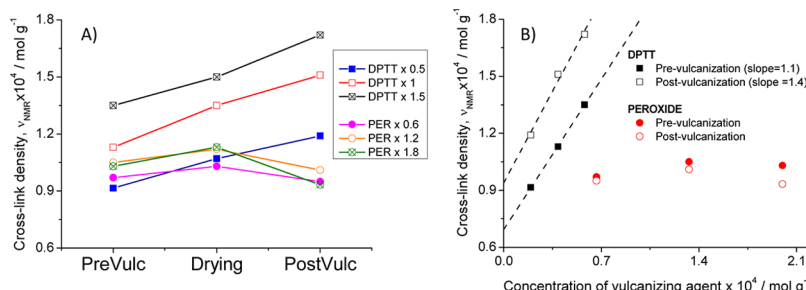


Figure 4. (A) Cross-linking density (ν) of various concentrations of DPTT and peroxide in the three different states: prevulcanization in latex state, drying and film formation, and postvulcanization in film state. (B) Efficiency of pre- and postvulcanization reactions for DPTT and peroxide as the relationship of cross-link density (measured by NMR) and the concentration of vulcanizing agent. Numbers in parentheses represent the slope of the linear fit for DPTT vulcanization processes.

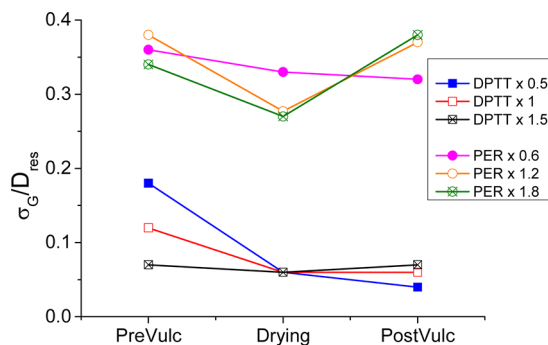


Figure 5. Variation of the relative width of the distribution of cross-link density (σ) to the average value (D_{res}) for all three different states. A Gaussian distribution of cross-link density was assumed.

understand this behavior, it is necessary to take into mind that the prevulcanization process depends on both diffusion of the vulcanizing agent inside the rubber particle and the subsequent cross-linking reaction. According to prevulcanization kinetics explored in Figure 2, the reaction rates in sulfur vulcanized samples are much slower than peroxide vulcanized samples. Consequently, the different reactive molecules have enough time to diffuse inside the rubber particles; hence, we observe the formation of homogeneous networks with increasing cross-link density according to the DPTT concentration (see Figure 6A). On the other hand, the reaction rate in peroxide vulcanization is very fast, where the cross-link density increases immediately after prevulcanization starts (see Figure 2). The time that peroxide molecules have to diffuse inside the rubber particle is reduced drastically before the cross-linking reaction starts. According to results shown in Figure 6A, the spatial distribution of cross-links on rubber particles (measured in latex state) for samples prevulcanized with peroxide are broader than the homogeneous network structures obtained with DPTT. The heterogeneous networks formed during peroxide prevulcanization consist of highly cross-linked areas in combination with slightly cross-linked or even un-cross-linked polymer segments. This structural evidence supports the formation of core–shell-like structures. Highly cross-linked surfaces of rubber particles slow down the diffusion process. This could be the main reason for the limited cross-link density measured in the peroxide-vulcanized samples in opposition to the sulfur system. Independent of the peroxide concentration, the final

network structure after prevulcanization process is almost the same in NR latex.

Film Formation and Postvulcanization Process. The drying process promotes the interparticle interaction and formation of coherent and continuous polymer film. Cross-linked rubber particles are packed, and some interactions between them could take place. It provokes the formation of additional topological constraints measurable by NMR, as was demonstrated by the y -intercept value in Figure 4B. At this point, it should be pointed out that the interfusion of cross-linked particles is restricted to roughly one network mesh size. Therefore, the additional topological constraints measured by NMR should take place mainly in the bulk volume of the latex spheres because of the film formation. Cooperation and/or packing between polymer chains reduce and homogenize their conformational space, playing a key role in the elastic properties of those materials because of the reduction in chain entropy. As a consequence, the spatial distribution of cross-links is narrower as compared with the prevulcanized rubber particles. This fact hides the differences observed in the spatial distribution of cross-links caused by the DPTT concentration, as shown in Figure 5.

It is important to remark that peroxide vulcanized samples always show broader spatial distributions of cross-links compared with DPTT samples, even after film formation (see Figure 6B). This heterogeneous network structure on polymer films is a direct consequence of core–shell structure formed during prevulcanization, and it seems to be independent of the peroxide concentration.

The postvulcanization process is a useful process in the latex industry because it accelerates the drying process and facilitates the rearrangement of polymer chains inside the films. However, it causes opposite consequences on the network structure according to the recipe used. This thermal process (130 °C for 30 min) applied on samples prevulcanized with peroxide seems to promote the reaction of remaining peroxide, creating radicals that enhance the natural sensitivity of NR to thermo-oxidative processes.¹⁵ It promotes chain scission reactions and, in consequence, a slight reduction in the cross-link density (with a higher effect with increasing peroxide concentration) and the broadening on the spatial distribution of cross-links (Figures 4 and 5).

On the opposite side, samples prevulcanized with DPTT show higher cross-link density and narrower spatial distribution

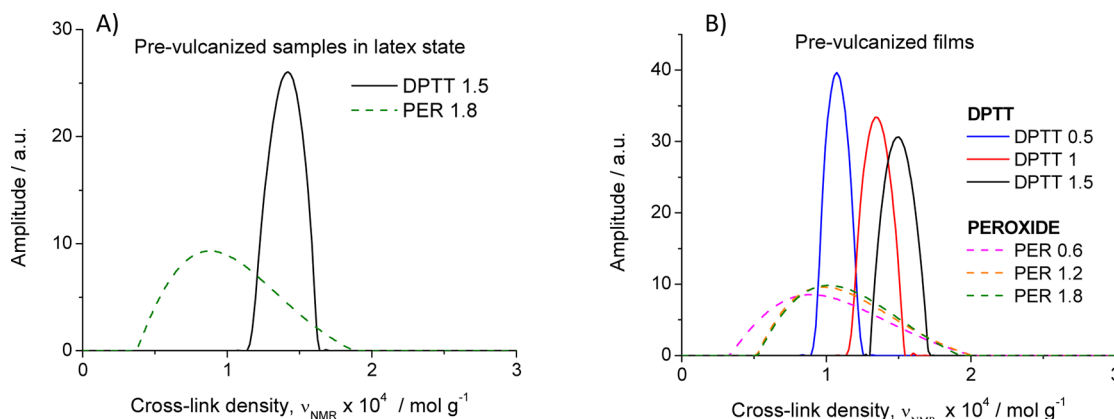


Figure 6. Actual spatial cross-link distribution for prevulcanized samples in latex state (A) and dried films (B) according to the regularization analysis of NMR data.

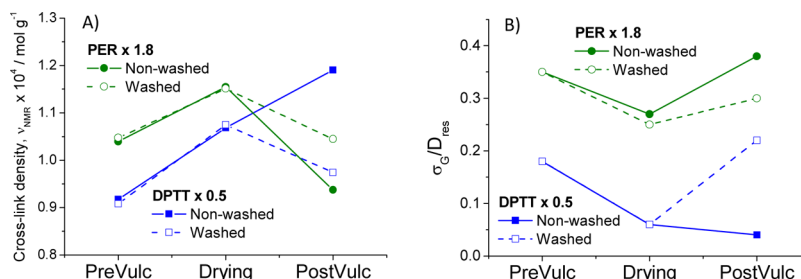


Figure 7. Effect of washing the excess of curing agent on the cross-linking density (A) and relative width of spatial cross-links distribution (B) in the three different states: prevulcanization in latex state, drying and film formation, and postvulcanization in film state.

after postvulcanization processes as compared to prevulcanized samples. It seems to indicate that postvulcanization promotes both the inter-rearrangement of polymer chains in NR films and also the chemical interactions between rubber chains because of the reaction with the remaining DPTT (unreacted DPTT molecules after the prevulcanization process). Postvulcanization enhances the efficiency on the cross-linking reaction and achieves values close to 1.4 mol of cross-links per mole DPTT without modifying the homogeneity of the formed networks (see Figures 4 and 5). The lack of evidence that supports the well-known thermo-oxidative aging on NR has to be directly related to the presence of antioxidants (e.g., Wingstay-L) in those samples prevulcanized with DPTT.

This important point was confirmed after the analysis of washed samples. For that purpose, prevulcanized latex was diluted to 30% dry rubber content (DRC) and stabilized with 1% w/v of sodium dodecyl sulfate (SDS), followed by centrifugation at 12 000 rpm for 40 min. The cream fraction was redispersed in distilled water. This procedure was repeated three times to clean the excess reacting agents (DPTT and peroxide) and antioxidants (Wingstay-L). It is important to point out that the washing procedure does not modify the network structure after prevulcanization nor during the film formation, as was demonstrated in Figure 7. Nevertheless, its effect is clear during postvulcanization. Figure 7 shows that washed samples (including those prevulcanized with DPTT) suffer a considerable degradation during postvulcanization. As a consequence, the cross-link density decreases and its spatial distribution becomes broader. Thermo-oxidative degradation in NR leads to chain scission reactions via a radical mechanism. In addition, thermolabile sulfidic cross-links (characteristics on samples vulcanized with DPTT) could also be affected. For that reason, the sample prevulcanized with DPTT seems to be more degraded after postvulcanization than the sample prevulcanized with peroxide. In any case, the natural tendency of NR to be degraded via thermo-oxidation processes emerges in the absence of antioxidants.

In conclusion, the postvulcanization process improves formation and drying of NR latex films, but they should be properly protected against thermo-oxidative degradation. In that case, the excess of vulcanizing agent, e.g. DPTT, promotes the formation of additional cross-links without affecting the quite homogeneous network structure obtained after prevulcanization. This is because cross-linking and degradation reactions are two competing processes where cross-linking is favored and is able to hide any effect caused by the degradation reaction on NR samples. Without protection against aging, postvulcanization has undesirable effects on the NR latex films.

On the opposite side, the excess of peroxide promotes formation of additional radicals that enhances the degradation

of NR during postvulcanization process. It leads to a complex network structure, since the original core-shell structure obtained after prevulcanization with peroxides becomes even more heterogeneous with lower cross-link density. Finally, it is important to remark on the difficulty to protect these samples against thermo-oxidative degradation with antioxidants because it could strongly affect the complex prevulcanization process via radical reactions.

Stress–Strain Relations. The stress–strain relations of pristine latex and heat treated pristine latex (130 °C for 30 min) are compared in Figure 8. The heat condition is the same

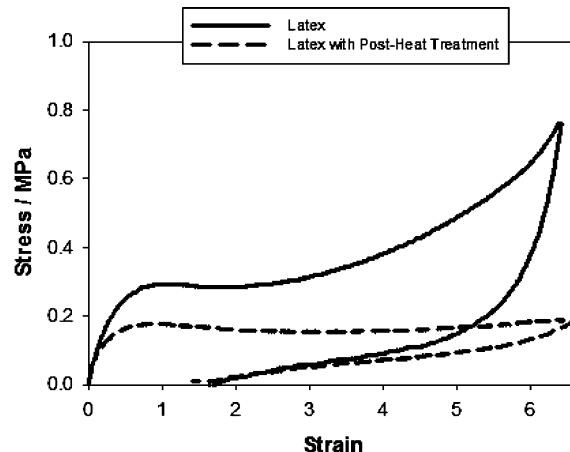


Figure 8. Stress–strain relationship during stretching and relaxation of latex and latex with post-heat treatment at 130 °C.

as the post vulcanization condition. The stress of pristine latex showed an upturn and increased significantly at the onset strain of 3.0, which may be attributed to the presence of the naturally occurring network structure. On the other hand, latex with post-heat treatment did not show the upturn of stress at large strain, indicative of the loss of an original network structure. Table 3 shows the 100% modulus, 300% modulus, and tensile strength for all the samples. For the pristine latex, the modulus and tensile strength decreased with the post-heat treatment at 130 °C for 30 min. Since no antioxidants were added to this sample, the post-heat treatment at 130 °C provoked the thermo-oxidative aging of NR, where it may cause chain scission reactions (shown in Figure 7), and the decomposition of proteins and phospholipids, leading to the destruction of network points. The literature suggested that the removal of proteins and phospholipids destroyed the naturally occurring network, resulting in significant decreases in tensile properties.¹⁶

Table 3. 100% Modulus, 300% Modulus, and Tensile Strength of Unvulcanized and Vulcanized (Both DPTT and Peroxide) Latex Samples at Various Concentrations and Post-Heat Treatment 130 °C

sample	100% modulus (MPa)	300% modulus (MPa)	tensile strength (MPa)
latex	0.29	0.32	0.76
latex PostV	0.18	0.15	0.19
DPTT 0.5	0.41	0.74	3.95
DPTT 1.0	0.49	0.93	5.14
DPTT 1.5	0.59	1.11	6.60
DPTT 0.5 PostV	0.37	0.60	3.07
DPTT 1.0 PostV	0.51	0.86	5.10
DPTT 1.5 PostV	0.62	1.22	6.86
Per 0.6	0.41	0.66	3.27
Per 1.2	0.42	0.81	4.36
Per 1.8	0.40	0.72	3.74
Per 0.6 PostV	0.27	0.56	1.68
Per 1.2 PostV	0.33	0.80	2.00
Per 1.8 PostV	0.30	0.65	1.43

The prevulcanized samples used for measurements include the prevulcanization and drying/film formation processes after film formation; since prevulcanization takes place in the solution phase, we cannot measure the mechanical properties of real prevulcanized rubber samples.

The stress-strain curves of prevulcanized latex and postvulcanized latex for the different concentrations of DPTT are shown in Figure 9. The absolute stress values of the sulfur-

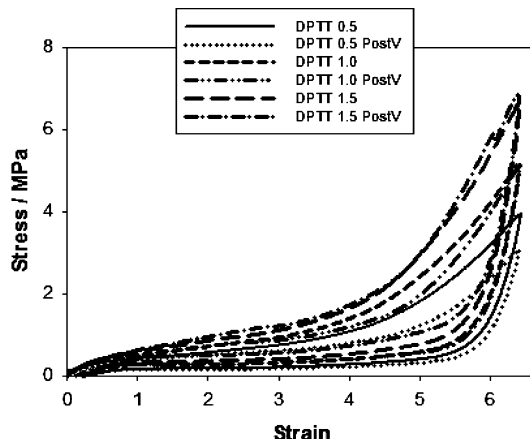


Figure 9. Comparison of the stress-strain relations of pre- and postvulcanized latex with various concentrations of DPTT.

vulcanized samples are much larger (almost 10 times greater) than the unvulcanized pristine NR latex. These sulfur-vulcanized samples are not affected by the thermal aging of the naturally occurring network because it was properly protected via the addition of antidegradants. As shown in Figure 9, the stress-strain curve of sulfur-vulcanized latex showed a hysteresis, which was typically found in pure vulcanized natural rubber. The presence of network structure was confirmed with the upturn of stress at large strains. The absolute stress during retraction was much smaller than during stretching. This is attributed to the presence of stable crystallites that were formed during stretching. With increasing DPTT concentration, there was an increase in the modulus and tensile strength as shown in Table 3. This is in agreement with

our DQ NMR measurements that at higher sulfur concentrations there was an increase in the cross-linking density and more network points were formed.

At low concentrations of DPTT, prevulcanized latex with DPTT has higher modulus and tensile strength than postvulcanized latex. However, at higher concentrations of DPTT, the modulus and tensile strength of pre- and postvulcanized latex are almost identical. The main difference between prevulcanization/film formation and postvulcanization is the slight increase in cross-link density because of the thermal treatment (as it was demonstrated by the DQ NMR experiments). Since the modulus and tensile strength of the pre- and postvulcanization are almost identical, this is an indication that slight variations on the network structure caused by the postvulcanization process have no relevant effects on the mechanical properties of those samples.

Figure 10 shows the stress-strain curves of prevulcanized latex and postvulcanized latex for the different concentrations

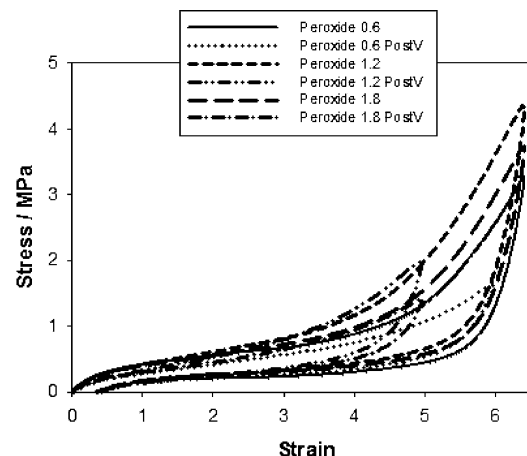


Figure 10. Comparison of the stress-strain relations of pre- and postvulcanized latex with various concentrations of peroxide.

of peroxide. A hysteresis is also observed similar to that observed in sulfur vulcanized samples. The stress-strain relations are independent of the concentration of peroxide, which is in agreement with our DQ NMR measurements. Peroxide vulcanization may create a core–shell-like structure that reduces the diffusion of vulcanizing agents to the inside of the latex particles; hence, the cross-link density is unchanged even at higher concentrations. It is to be noted that the postvulcanized samples with 1.2 and 1.8 phr of peroxide are stretched only up to strain 5 instead of 6. The modulus at small strain did not change by postvulcanization. The modulus and tensile strength are larger in prevulcanized than postvulcanized samples. The additional thermal treatment in postvulcanized peroxide samples may have caused chain scission reactions that reduced the cross-link density and increased the broadening of cross-link spatial distribution.

WAXD (Wide-Angle X-ray Diffraction) Patterns. WAXD of unvulcanized and vulcanized samples (both pre- and postvulcanized) are measured simultaneously under deformation. Figure 11 shows selected two-dimensional WAXD patterns of latex, latex with post-heat treatment at 130 °C, pre- and postvulcanized latex with 2.25 phr of DPTT (labeled as DPTT 1.5 and 1.5 PostV, respectively), and pre- and postvulcanized latex with 1.8 phr of peroxide (labeled as Per 1.8 and Per 1.8 PostV, respectively) during stretching. For

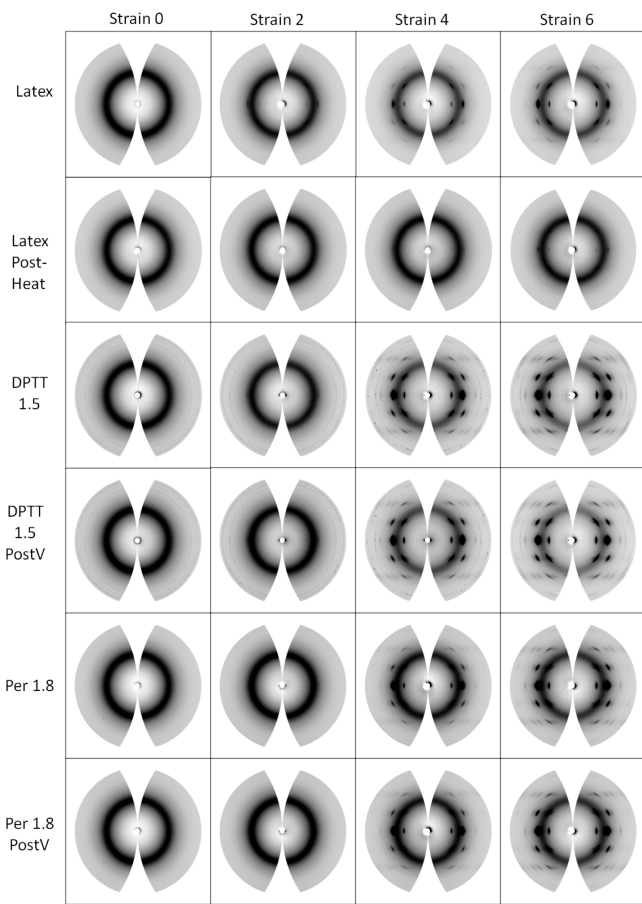


Figure 11. Selected two-dimensional WAXD patterns of latex, latex with post-heat treatment at 130 °C, pre- and postvulcanized latex with 2.25 phr of DPTT (labeled as DPTT 1.5 and 1.5 PostV, respectively), and prevulcanized latex with 1.8 phr of peroxide (labeled as Per 1.8 and Per 1.8 PostV, respectively) during stretching.

the pre- and postvulcanized samples with various concentrations of DPTT and peroxide, the WAXD patterns at each concentration were all similar and only the 2.25 phr DPTT and 1.8 phr peroxide are shown in the figure. An intense halo was

observed both prior and during stretching. This halo is attributed to amorphous chains with no preferred orientation that was present prior to stretching and remained throughout stretching. Furthermore, highly oriented crystalline reflection peaks are observed at higher strains that were not observed prior to stretching at strain 0, indicating the occurrence of strain-induced crystallization (SIC).

Figure 12 shows the integrated intensities of the two-dimensional WAXD patterns for latex, latex with post-heat treatment, pre- and postvulcanized latex with 2.25 phr of DPTT, and pre- and postvulcanized latex with 1.8 phr of peroxide at strains 2 and 6. The intensities of the crystalline reflections increase with strain during stretching. The intensities of the amorphous halo decrease only slightly during stretching, indicating the persistence of sizable amorphous chains in the highly stretched sample. As reported in the literature by Toki et al.,¹ during deformation of natural rubber, up to 75% of polymer chains remain in the unoriented state even at large strains, around 20% of chains are in the crystalline state, and 5% of the molecules are in the oriented amorphous state.

Figure 13 shows the crystallinity fraction for all the samples as a function of strain. For pristine latex, the crystallinity fraction is lower for the latex with post-heat treatment at 130 °C. This is consistent with the previous stress-strain relation results, where the high temperature may have caused the destruction of the naturally occurring network, which is necessary for the induction of crystallite formation.

In vulcanized latex with DPTT, more amorphous chains were oriented during stretching and an increase in crystallinity fraction was observed. Furthermore, the crystallinity fraction increased with concentration of DPTT. This is in agreement with previous DQ NMR and stress-strain relation results, where the increase in sulfur concentration led to an increase in the cross-linking density and more network points were formed. As shown in Figure 13, for all the concentrations of DPTT, postvulcanized latex has only a slightly higher crystallinity fraction than prevulcanized (and dried) latex films. This demonstrates that small changes on cross-link density during the postvulcanization process do not have any effect on the strain-induced crystallization or on the mechanical properties of these samples. The further thermal treatment led

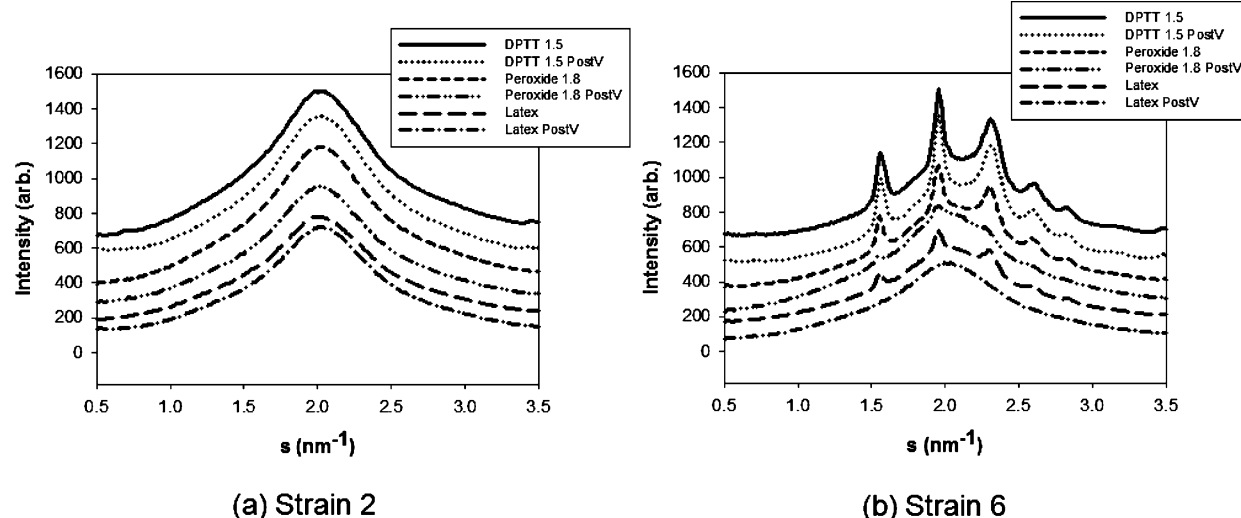


Figure 12. Integrated intensities of the two-dimensional WAXD patterns for latex, latex with post-heat treatment, pre- and postvulcanized latex with 2.25 phr of DPTT, and pre- and postvulcanized latex with 1.8 phr of peroxide at strains 2 (a) and 6 (b).

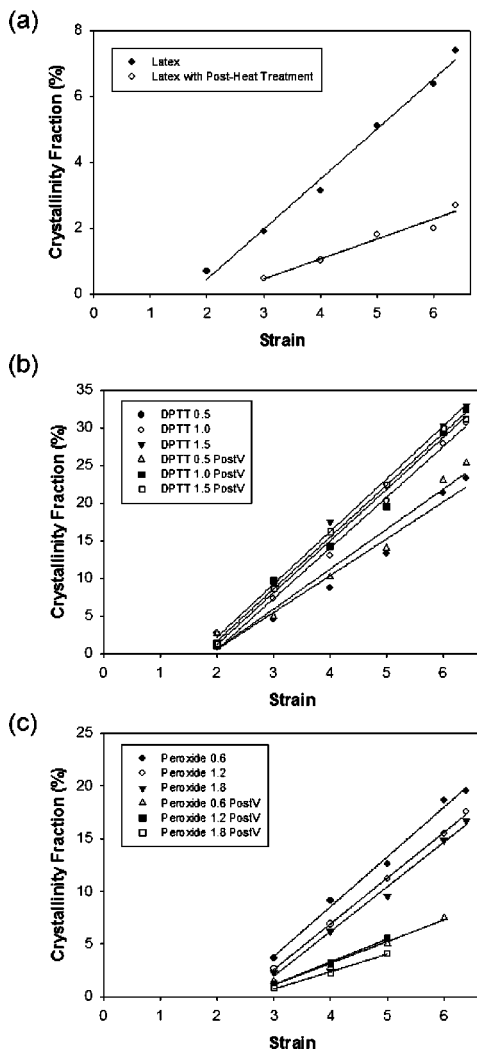


Figure 13. Crystallinity fraction with respect to strain for (a) latex and latex with post-heat treatment; comparison of crystallinity fraction between pre- and postvulcanization with (b) DPTT and (c) peroxide.

to the slight increase in cross-linking density and network points for postvulcanized latex and hence a slightly higher crystallinity fraction.

As for samples vulcanized with peroxide, the crystallinity fraction is independent of the concentration of peroxide, which is consistent with the DQ NMR and stress-strain relation results. Furthermore, the crystalline intensities are much weaker than the intensities observed for the samples vulcanized with DPTT. This may be attributed to the inhomogeneous network structure formed on NR samples after vulcanization with peroxide. The postvulcanized samples with peroxide have a smaller crystallinity fraction than the prevulcanized samples with peroxide, which is a consequence of the additional thermal treatment that might cause chain scission reactions and decrease the cross-linking density.

The onset strain of crystallization can be estimated from the best fit curve applied to each sample by extrapolating to the crystallinity at 0% position. It was found that the onset strain of crystallization of latex occurred much earlier than that of latex with post-heat treatment (strain 1.6 and 2.2 for latex and latex with post-heat treatment, respectively). Unvulcanized latex with post-heat treatment resulted in less network points, late development of crystals, and low crystallinity fractions. The

onset strain of crystallization of pre- and postvulcanized latex at all three concentrations of DPTT occurred at the same strain of around 1.8, which tells us that the onset strain of crystallization is independent of the concentration of sulfur and the small changes on cross-link density created during postvulcanization. The onset strain of crystallization of vulcanized latex samples with DPTT was slightly higher than the onset strain of crystallization of unvulcanized latex. This may be attributed to the bulky piperidine rings at the ends of DPTT that inhibit the extension of chains to form crystallites.

The onset strain of crystallization for prevulcanized latex with 0.6, 1.2, and 1.8 phr of peroxide is 2.23, 2.38, and 2.50, respectively. Unlike vulcanized samples with DPTT, the vulcanized samples with peroxide are dependent on concentration and temperature aging. With increasing concentration of peroxide, the onset strain of crystallization occurs at higher strains. Furthermore, the onset strain of crystallization occurs at larger strains for postvulcanized than prevulcanized samples. This could be attributed to the enhanced thermo-oxidative degradation of network due to the presence of unreacted peroxide during the postvulcanization process.

DISCUSSION

Prevulcanization with DPTT led to homogeneous network structures, whereas peroxide promotes core-shell structures that (after film formation) develop inhomogeneous network structures. The latter always show smaller crystallinity fractions with delayed onset strain of crystallization with respect to the homogeneous DPTT samples (always comparing samples with similar cross-link density). It demonstrates that in addition to cross-link density spatial distribution of cross-links is a central factor to understand strain induced crystallization of NR.

These NMR and *in situ* synchrotron X-ray diffraction results seem to be in contradiction with the conclusions described by Ikeda et al.¹⁷ in a previous study. On the basis of strain-induced crystallization (SIC) studies, these authors found differences in the onset of SIC behavior as a function of the cross-link density. These differences were explained on the basis of assuming very homogeneous structures for peroxide-cured NR, yet even bimodal structures for sulfur-cured NR. Nevertheless, in a most recent work¹⁸ based on small-angle neutron scattering measurements (SANS), they conclude that the structure of peroxide cross-linked NR is inhomogeneous and is composed of several kinds of clusters with different sizes. In the same way, strain-induced crystallization behavior of NR vulcanized with peroxide was then related to a progressive reduction of the overall size of inhomogeneities of these samples with the cross-link density. Therefore, apparent differences and contradictions between these studies could be transformed into complementary results in perfect agreement based on the studied length scales. SANS^{17,18} is used to detect inhomogeneities in the range of 20–50 nm. In sulfur-cured polyisoprene rubber (IR), such inhomogeneities may partially be due to ZnO clusters, as found by transmission electron microscopy (TEM).¹⁹ The present NMR study provides more local information since it is sensible to spatial cross-linking inhomogeneities on scales of several nanometers and above. The network structures are obtained directly by simultaneous molecular-scale observation of the behavior of all monomers in the rubber. They suppose clear experimental evidence about the link between the actual local rubber network structure and strain-induced crystallization without invoking any model.

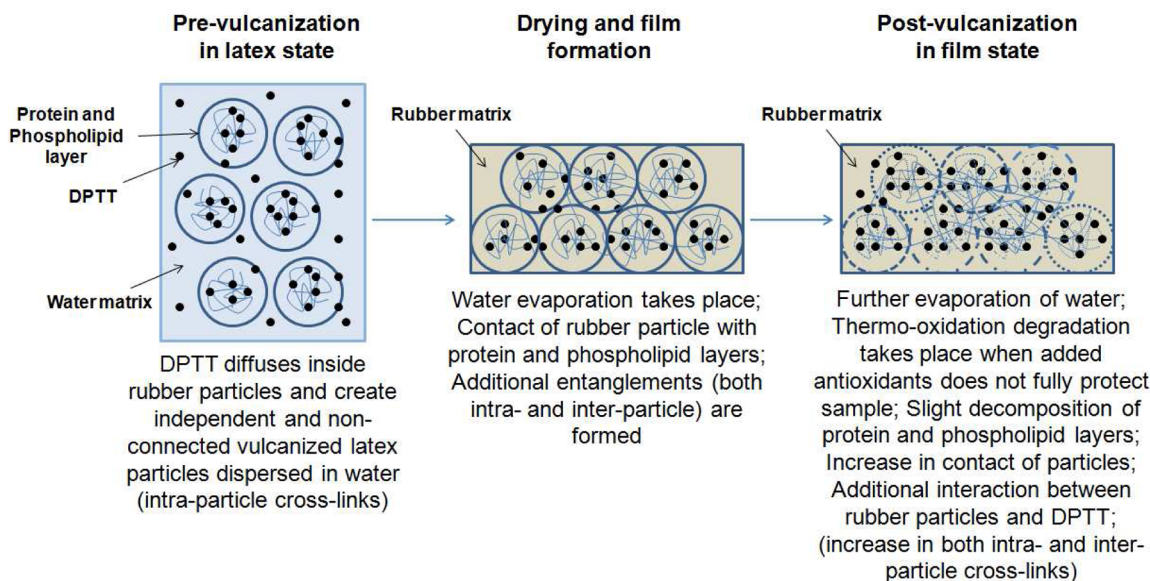


Figure 14. Schematic model of the three different states for vulcanized latex: prevulcanization in latex state, drying and film formation, and postvulcanization in film state.

It is possible to conclude that the NR samples vulcanized with sulfur exhibit a rather homogeneous rubber matrix down to very local scales, with inhomogeneities at larger scales arising from the nonrubber components. In contrast, vulcanization with peroxides always creates inhomogeneous network structures on all scales because of radical reactions. These differences on the local network structure led to variations on more complex phenomena like strain-induced crystallization.

Figure 14 shows a schematic model of the different states using DPTT as the vulcanizing agent: prevulcanization in latex state, drying and film formation, and postvulcanization in film state. During prevulcanization, latex particles are dispersed in water. DPTT diffuse inside the rubber particles and then react with the rubber chains. Cross-linking reaction of rubber particles takes place inside each individual rubber particle (intraparticle cross-link density), creating independent and nonconnected vulcanized rubber particles. During this process, the protein and phospholipid layers stabilize the rubber particles dispersed in water.

During drying and film formation, water evaporation plays a significant role in network formation. As water evaporates to form a film, rubber particles come in contact with each other and additional entanglements and cross-linking reaction takes place between rubber particles (interparticle cross-link densities), which are not seen in NMR due to their low volume fraction. According to Figure 4, during film formation, slight increases in the cross-linking density as compared to prevulcanization in the latex state were observed. According to previous DQ NMR results, interparticle constraints (entanglements and cross-links) and chain rearrangements created during film formation homogenize the conformational space of rubber chains. This fact tends to create a continuous rubber media, where proteins and phospholipids are pushed away from the particle boundaries, creating aggregates. Nevertheless, the chain ends on the highly cross-linked particles (during the prevulcanization process) usually show higher difficulties to diffuse out the original particle to interact with the neighbor particle. In this case, rubber particles retain the particle shape after film formation (SEM images are not shown). This step

should be strongly influenced by the network structure developed on the individual rubber particles as it was suggested by atomic force microscopy.²⁰ It is of central importance to correlate the network structure after prevulcanization (e.g., perfect homogeneous network structure in DPTT samples or core–shell structures in peroxide samples) with the formation and evolution of polymer films. The main inconvenience to develop this investigation was lack of experimental techniques to analyze the rubber network structure on latex state. Nevertheless, time-domain NMR experiments have shown their potential to overcome this problem and reveal the actual network structure on latex state. It will take part in an upcoming study.

During postvulcanization in the film state, the high temperature (130 °C for 30 min) promoted film drying, and in addition, it caused further interactions between rubber particles and additional reaction of DPTT. In this case, samples were protected (by addition of antioxidants) against the thermo-oxidation, and consequently, an increase in intraparticle cross-links and interparticle cross-links takes place as compared to the drying/film formation state. In addition, the high temperature may have caused the decomposition of protein and phospholipid layers, and therefore, it makes easier the interactions between particles. According to Figure 4, the cross-link density is higher than the prevulcanization and drying states. Overall, drying from latex state to dry films improved the homogeneity of the samples and promoted the creation of new interactions.

CONCLUSION

The combination of ¹H DQ NMR and WAXD experiments provided us with quantitative information regarding rubber network structure along the different steps on the usual manufacturing procedure of NR latex. It consists of three different states: prevulcanization in latex state, drying and film formation, and postvulcanization in film state. These three states play a large role in the overall vulcanization process, and they can affect both network structure and mechanical properties. From DQ NMR and synchrotron X-ray results, a

schematic model for each of these processes was proposed. The network structure at each of these states was correlated with its physical properties.

In this sense, time domain NMR experiments have been shown as an easy and quantitative tool to overcome the lack of experimental techniques to characterize the network structure of individual rubber particles that conform the NR latex. ^1H DQ NMR experiments, performed on inexpensive and easy-to-use low-field spectrometers, were used to obtain qualitative information about the prevulcanization kinetics and the actual network structure of rubber particles dispersed on water. It promotes this experimental approach as valuable methodology to be applied in basic research on academic and technological developments in the industry.

Unvulcanized latex (without any additive) and latex heated at 130 °C for 30 min (similar to postvulcanization process) were tested in order to analyze the intrinsic thermal behavior of NR without the interference of any chemicals. Latex after the thermal treatment always shows lower mechanical properties and crystallization fraction than latex due to high-temperature degradation of polymer chains, proteins, and phospholipids. Chain scission may reduce the molecular weight of macromolecules, whereas removal of proteins and phospholipids may destroy the naturally occurring network, resulting in significant decreases in tensile properties.

NR latex vulcanized with the sulfur donor DPTT always shows better elastic properties (higher modulus and tensile strength) than those samples vulcanized with peroxides. In pre- and postvulcanized latex with DPTT, an increase in the DPTT concentration led to more network points with extremely narrow spatial distribution. As a consequence, an increase in modulus and crystal fraction was observed. According to these results and prevulcanization kinetics, it was demonstrated that cross-linking reaction of DPTT is slow enough to allow the diffusion of vulcanizing agent inside the rubber particle. It promotes the formation of a highly homogeneous rubber network with excellent physical properties.

On the opposite hand, the peroxide vulcanization process occurs very fast. The diffusion of the vulcanizing agent into the latex particle is limited where vulcanization takes place on the surface. This creates a core–shell like structure that prevents additional peroxide to penetrate into the latex particle. For these reasons, pre- and postvulcanized latex with peroxide show lower crystallinity fraction (independent of the concentration of peroxide) that affect the stress–strain properties.

Film formation enhances the interparticle interactions and formation of additional topological constraints between polymer chains without the assembly of chemical cross-links. It increases the dynamic order parameter (related with the lower entropy on the system) and homogenizes the segmental conformational space as compared with the prevulcanized rubber particles. Drying process and film formation is usually enhanced by postvulcanization treatment at higher temperatures. That effect is shown by postvulcanized latex with DPTT that has slightly higher cross-linking density, mechanical properties, and crystallinity fraction than prevulcanized latex. In this case, the slight improvement is caused by two positive effects: the addition of antioxidant minimizes the natural aging tendency of NR and the further reaction of (unreacted) DPTT increases the cross-link density without changing the narrow spatial distribution.

By comparing pre- and postvulcanized latex with peroxide, prevulcanized latex with peroxide has a higher cross-linking

density, mechanical property, and crystallinity fraction than postvulcanized latex. In these samples without antioxidant protection, the additional thermal treatment for postvulcanization led to negative effects on network structure and elastic properties. Reaction of peroxide in excess facilitates the chain scissions of NR that resulted in a decrease in cross-link density.

Improved elastic properties on latex samples seem to be directly related with formation of homogeneous network structures that facilitates the strain-induced crystallization of NR. To achieve that objective, it is important to select the proper recipe (e.g., vulcanizing systems that allow diffusion inside rubber particles before cross-linking reaction and addition of antioxidants) and optimized pre- and postvulcanization conditions (time and temperature). Application of time-domain NMR facilitates and rationalizes this complex work, giving quantitative information about the actual network structure in every step of latex manufacturing. Network structure in sulfur vulcanized latex is rather homogeneous than peroxide vulcanized one, though previous NMR studies using ^{13}C and deuterium on vulcanized NR reported that carbon-filled vulcanized compounds seem to be homogeneous^{21,22} and oriented rubber chains in vulcanized pure compounds are aligned with the stretched direction at less than 200% strain.^{23,24}

■ AUTHOR INFORMATION

Corresponding Author

*E-mail: shigeyikitoki@gmail.com (S.T.); jvalentin@ictp.csic.es (J.L.V.).

Notes

The authors declare no competing financial interest.

■ ACKNOWLEDGMENTS

J.C., S.T., L.R., and B.S.H. are financially supported by the National Science Foundation (DMR-0906512) and CICYT (MAT 2011-23476). J.L.V. thanks Secretaría de Estado de Investigación, Desarrollo e Innovación (Spain) for his Ramon y Cajal contract, and A.N. gives thanks for the financial support from Royal Golden Jubilee (RGJ) Ph.D. program (PHD/0257/2550).

■ REFERENCES

- (1) Toki, S.; Sics, I.; Ran, S.; Liu, L.; Hsiao, B. S.; Murakami, S.; Senoo, K.; Kohjiya, S. *Polymer* **2003**, *44*, 6003–6011.
- (2) Toki, S.; Sics, I.; Ran, S.; Liu, L.; Hsiao, B. S.; Murakami, S.; Senoo, K.; Kohjiya, S. *Macromolecules* **2002**, *35*, 6578–6584.
- (3) Keddie, J.; Routh, A. *Fundamentals of Latex Film Formation: Processes and Properties*; Canopus Academic Publishing Limited: Bristol, UK, 2010.
- (4) Perrellaa, F.; Gaspari, A. *Methods* **2002**, *27*, 77–86.
- (5) Amnuayponsri, S.; Sakdapipanich, J.; Tanaka, Y. *J. Appl. Polym. Sci.* **2009**, *111*, 2127–2133.
- (6) Saalwachter, K. *Prog. Nucl. Magn. Reson. Spectrosc.* **2007**, *51*, 1–35.
- (7) Valentín, J. L.; Posadas, P.; Fernandez-Torres, A.; Malmierca, M. A.; Gonzalez, L.; Chasse, W.; Saalwachter, K. *Macromolecules* **2010**, *43*, 4210–4222.
- (8) Chasse, W.; Valentín, J. L.; Genesky, G. D.; Cohen, C.; Saalwachter, K. *J. Chem. Phys.* **2011**, *134*, 044907.
- (9) Lewis, A. Accelerator DPTT, AkroChem Corporation, 2009.
- (10) Valentín, J. L.; López, D.; Hernández, R.; Mijangos, C.; Saalwachter, K. *Macromolecules* **2009**, *42*, 263–272.
- (11) Vaca-Chavez, F.; Saalwachter, K. *Phys. Rev. Lett.* **2010**, *104*, 198305.

- (12) Vaca-Chavez, F.; Saalwachter, K. *Macromolecules* **2011**, *44*, 1560–1569.
- (13) Saalwachter, K.; Gottlieb, M.; Liu, R.; Oppermann, W. *Macromolecules* **2007**, *40*, 1555–1561.
- (14) Posadas, P.; Fernández-Torres, A.; Valentín, J. L.; Rodríguez, A.; González, L. *J. Appl. Polym. Sci.* **2010**, *115*, 692–701.
- (15) Lemayev, N. V.; Kurbatov, V. A.; Liakumovich, A. G. *Polym. Sci. URS* **1981**, *23*, 419–425.
- (16) Amnuaypornsri, S.; Sakdapipanich, J.; Toki, S.; Hsiao, B. S.; Ichikawa, N.; Tanaka, Y. *Rubber Chem. Technol.* **2008**, *81*, 753–766.
- (17) Ikeda, Y.; Yasuda, Y.; Hijikata, K.; Tosaka, M.; Kohjiya, S. *Macromolecules* **2008**, *41*, 5876–5884.
- (18) Suzuki, T.; Osaka, N.; Endo, H.; Shibayama, M.; Ikeda, Y.; Asai, H.; Higashitani, N.; Kokubo, Y.; Kohjiya, S. *Macromolecules* **2010**, *43*, 1556–1563.
- (19) Dohi, H.; Horiuchi, S. *Polymer* **2007**, *48*, 2526–2530.
- (20) Ho, C. C.; Khew, M. C. *Langmuir* **2000**, *16*, 2436–2449.
- (21) Rault, J.; Marchal, J.; Judeinstein, P.; Albouy, P. A. *Macromolecules* **2006**, *39*, 8356.
- (22) Dupres, S.; Long, D. R.; Albouy, P. A.; Sotta, P. *Macromolecules* **2009**, *42*, 2634.
- (23) Kimura, H.; Dohi, H.; Kotani, M.; Matsunaga, T.; Yamauchi, K.; Kaji, H.; Kurosu, H.; Asakura, T. *Polym. J.* **2010**, *42*, 25–30.
- (24) Kameda, T.; Asakura, T. *Polymer* **2003**, *44*, 7539–7544.